Intermediate mass fragment yields from fusion and non-fusion processes in nucleus-nucleus collisions in Fermi energy domain: An integrated dynamical approach

C. Bhattacharya, S. Bhattacharya, and K. Krishan
Variable Energy Cyclotron Centre, 1/AF, Bidhan Nagar, Calcutta 700 064, India
(Received 17 September 1993)

Fusion and non-fusion contributions to the intermediate mass fragment yields in nucleus-nucleus collisions near the Fermi energy domain have been calculated in the framework of an integrated theoretical model where the dynamical evolution of the colliding system leads to the formation of either incompletely fused composite or incomplete deep inelastic and-or quasielastic fragments, which subsequently undergo statistical binary decay to yield final fragments. Salient features of incomplete fusion and incomplete deep inelastic collision processes have been studied in detail. Predicted yields from the incomplete fusionlike and non-fusionlike processes agree well with the respective experimental data. Calculated total elemental yields of the primary fragments also compare well with the experimental data in the whole range of intermediate mass fragments emitted in the Fermi energy domain. It has been observed that the secondary deexcitation of the primary fragments does not affect the total elementary yield distribution in a significant way.

PACS number(s): 25.70.Gh, 25.70.Jj

I. INTRODUCTION

The emission of intermediate mass fragments (IMF's, $3 \leq Z \leq 25$) in low-, intermediate-, and high-energy nucleus-nucleus collisions has been a subject of intense theoretical as well as experimental investigations in the recent years. In case of high-energy ($E/A \geq 100$ MeV/u) collisions at low-impact parameters, there are some indications [1–3] that the fragments may be emitted through "true" or instantaneous multifragmentation. In contrast, at low energies ($E/A \leq 10$ MeV/u), nuclear mean field plays the most crucial role and IMF emission is believed to be almost entirely due to asymmetric binary fragmentation process [4,5], resulting from the dynamical deformation of the nuclear mean field. Therefore, in the intermediate-energy domain, there is likely to be a transition from the binary fragmentation to the true multifragmentation. The relative importance of the two processes so far as the IMF emission in this energy domain is concerned, is an interesting question which is yet to be settled theoretically [6]. Detailed microscopic Vlasov-Uehling-Uhlenbeck [7], Boltzmann-Nordheim-Vlasov [8], or quantum molecular-dynamics [9] calculations are expected to shed some light on this problem. However, such calculations are often prohibitive because of their inherent complexity as well as their computer time requirements. Besides, for incident energies in and around the Fermi energy domain, nuclear mean field, though considerably weakened, plays a crucial role for the evolution of the nuclear dynamics. Consequently, the binary fragmentation process would have a significant contribution to the IMF emission and it may not be easily differentiated from other competing processes, i.e., instantaneous multifragmentation. Thus a systematic estimation of IMF emission through asymmetric binary fragmentation in the framework of a simple realistic model which incorporates the basic physics of nucleus-nucleus collision in the Fermi energy domain, is quite useful and such calculations may help in understanding, at least qualitatively, the degree of overlap between various competing processes in this energy domain. However, such systematic model calculations are, to the best of our knowledge, not available in the literature.

It is now well established that in nucleus-nucleus collisions with incident energies less than 10 MeV/u, the dominant mode of reaction is complete fusion, where the total incoming linear momentum and available energy is deposited into the fused composite system (compound nucleus). With the increase in bombarding energy $E/A > 10$ MeV/u, the phenomenon of incomplete fusion starts showing up and gradually takes over the complete fusion process [10,11]. In incomplete fusion process, light particles emitted in the initial phase of the reaction carry away a fraction of the linear momentum and energy from the entrance channel [12–15] and the remaining parts of the target and projectile fuse together to form an incompletely fused composite (IFC). The fused composite thus formed (through complete or incomplete fusion) then deexcites statistically through evaporation and-or binary fragmentation leading to the emission of two heavy fragments. Each of the fragments emitted at any step may in the next step undergo further binary division into two fragments and-or light particle evaporation and the process continues until the excitation energy remaining in the fragments is insufficient for their subsequent decay.

Apart from the above-mentioned process of sequential binary decay of the fused composite, which is predominant for central and near-central collisions leading to fusion, there are also significant contributions from peripheral collisions, i.e., quasielastic (QE) and deep in-

elastic (DI) processes which does not lead to the fusion of the reactants. In the intermediate-energy domain (10 MeV/u$\leq E/A \leq$100 MeV/u), non-fusion processes, especially the deep inelastic collision processes, are also "incomplete" in the sense that the excitation energy deposited in the fragments emitted in these reactions are significantly smaller than the total kinetic-energy loss from the entrance channel. These processes, where a fraction of the entrance channel kinetic energy is carried away by preequilibrium emission and which thereby causes a reduction of the intrinsic excitation of the fragments, are called incomplete deep inelastic collision (INDIC) processes. Similar incompleteness should also be observed for quasielastic reactions. However, for quasielastic processes, which are extremely peripheral in nature, preequilibrium emission drops down considerably, and intrinsic excitation of the fragments are also small; therefore, the effect of "incompleteness" may not be quite significant in this case. It is therefore evident that systematic theoretical studies of "incomplete" QE and DI reactions are also necessary for a proper understanding of the IMF production scenario in the intermediate-energy regime. This, to the best of our knowledge, has not been done in the past, although such systematic studies of incomplete fusion reactions are available in the literature [16]. Moreover, realistic estimation of the physical quantities that characterize the fused composite becomes quite complicated in the intermediate-energy regime with the onset of incomplete fusion. Because of the preequilibrium emission of fast particles which carry away significant amounts of energy, linear and angular momenta [17], the composite formed in incomplete fusion reactions is not uniquely defined as in the case of complete fusion reactions; instead, each of the observables, e.g., mass, charge, angular momentum, and excitation energy of the incompletely fused composite will have a distribution [16] which has to be properly taken care of for the subsequent decay of the composite. Similarly, the relevant observables for QE and DI primary fragment formed in peripheral reaction (non-fusion) will have some distribution because of the nucleon exchange between the reactants and preequilibrium emission. It is evident from the above discussion that entrance channel dynamics of the nucleus-nucleus collisions plays a vital role and must be properly incorporated in the theory for a proper understanding of the IMF emission near the Fermi-energy domain. Here we present an integrated dynamical model [18], where the evolution of the colliding system leads to the formation of incompletely fused composite (fusion) or to DI and QE fragments (non-fusion). Subsequent decay of these primary fragments leads to the production of the IMF's. The absolute individual contributions of fusion and non-fusion processes to the production of IMF's are calculated.

This paper is arranged as follows. The model along with the necessary details is described in Sec. II. In Sec. III, salient features of the present model are discussed along with the numerical results. Comparison of the present model predictions with the experimental data for some representative systems is also made in Sec. III. Finally the summary and conclusions are given in Sec. IV.

II. THE MODEL

The model basically consists of two parts: (i) the calculation of the initial dynamical phase or the preequilibrium phase and (ii) the calculation of the subsequent equilibrium binary fragmentation phase. In the initial dynamical phase, the time evolution of the dinuclear complex formed in nucleus-nucleus collisions is followed until there is no more preequilibrium emission. At the end of this phase, the system is assumed to be equilibrated leading to the formation of incompletely fused composite for the central collisions or to the production of deep inelastic, quasielastic fragments for the peripheral collisions. In the next phase, the hot composite and the primary DI and QE fragments are allowed to decay statistically through evaporation and/or binary fragmentation to yield the final fragments. The initial dynamical phase of the reaction is characterized by the emission of fast particles or promptly emitted particles (PEP's) throughout the temporal phase of the evolution of the dinuclear complex. For the time evolution of this initial phase, semiclassical trajectories for each impact parameter are generated by solving Euler-Lagrange equations. In the trajectory calculation the conservative forces are the nucleon proximity and Coulomb forces; the nonconservative frictional forces are generated self-consistently using stochastic nucleon exchanges. The trajectory calculation is started when the two nuclei come closer than a critical distance [17] where the densities of the two reactants start overlapping and is stopped at the time when there is no further preequilibrium emission. This time is typically $\sim$50 fm/c.

A. Preequilibrium phase

For the calculation of preequilibrium emission, we have employed the generalized version of the promptly emitted particle model [17]. The transport of nucleons through the window formed at the interface where the two densities overlap and subsequent particle emission in the continuum form the basis of the model. When a nucleon is exchanged stochastically from nucleus A (donor) to nucleus B (recipient), its energy in the recipient (ε_b) boosted by coupling of relative velocity $\vec{v}_{\rm rel}$ and the intrinsic Fermi velocity $\vec{v}_a$ is given by

$$\varepsilon_b = 1/2\ m(\vec{v}_a + \vec{v}_{\rm rel})^2\ , \tag{1}$$

where m is the nucleon mass. The transfer of a single nucleon from the nucleus A to the nucleus B induces an elementary hole excitation ΔE_h^A in the donor nucleus and a particle excitation ΔE_p^B in the recipient nucleus. The quantities ΔE_h^A and ΔE_p^B are given by

$$\Delta E_h^A = E_F - 1/2\ mv_a^2\ , \tag{2a}$$

$$\Delta E_p^B = 1/2\ m(\vec{v}_a + \vec{v}_{\rm rel})^2 - E_F + \omega\ . \tag{2b}$$

The corresponding angular momenta transfer $\vec{j}_h^A$, $\vec{j}_p^B$ are given by

$$\vec{j}_p^B = m\vec{r}_b \times (\vec{v}_a + \vec{v}_{\rm rel}), \tag{2c}$$

$$\vec{j}_h^A = -m(\vec{r}_a \times \vec{v}_a) \ , \tag{2d}$$

where E_F is the Fermi energy and ω is the driving force per nucleon transfer and $\vec{r}_a$, $\vec{r}_b$ are the position vectors of the point on the common window plane measured from the centers of the nuclei A and B, respectively. The transferred nucleon has to overcome a barrier at the interface: Coulomb plus nuclear for the protons and only nuclear for the neutrons. The effect of the driving forces caused by potential-energy surfaces on the nucleon transfer is also properly taken care of. A shell-corrected macroscopic driving force derived from the liquid-drop model, is used in the present calculation. The one-way transfer of nucleons from the nucleus A to the nucleus B between the time interval t and $t + \Delta t$ is then given by

$$\mathcal{N}_{AB}(t)\Delta t = \mathcal{A}(t)\eta(\vec{v}_a + \vec{v}_{\rm rel})f(\varepsilon_A, T_A)\bar{f}(\varepsilon_B, T_B)\mathcal{T}\Delta t \ , \tag{3}$$

where $\mathcal{A}(t)$ is the window area at time t: η is the bulk flux; f, $\bar{f}$ are the occupancies and nonoccupancies in nucleus A and nucleus B having instantaneous temperatures T_A and T_B; and $\mathcal{T}$ is the barrier penetration factor calculated using Hill-Wheeler formula, assuming the barrier to be an inverted parabola in the neighborhood of the maximum. The time step Δt is chosen such that the transferred flux $\mathcal{N}_{AB}(t)\Delta t$ is small compared to unity. In reality, in each time step, either a single nucleon is transferred (multiple nucleon transfer probability is negligible) or there is no transfer at all. The transfer is simulated through the generation of random numbers: if $\mathcal{N}_{AB}(t)\Delta t$ is greater than or equal to the random number, a particle transfer is realized. The transferred nucleon may either suffer two-body collision with the inmedium nucleons and be absorbed in the recipient nucleus, or be emitted as a prompt particle (one-body PEP's) if its kinetic energy satisfies the condition

$$\varepsilon_b > U + V_C, \tag{4}$$

where U is the depth of the nucleon potential and V_C is the Coulomb barrier (zero for neutrons). The absorption probability of the transferred nucleon in the recipient is $(1 - e^{-d/\lambda})$, where d is the path length in the recipient and λ is the energy-dependent mean free path of the nucleon [17]. However, in the intermediate-energy domain, after the first two-body collision, either one or both of the scattered nucleons may have sufficient energy so that energy condition [Eq. (4)] is satisfied and they may also be emitted in the continuum (two-body PEP's). As a consequence, particle absorption in the recipient is further attenuated (taken as e^{-d_i/λ_i}, i=1,2). The probability $e^{-d/\lambda}$ is treated against a random number. If the probability is greater than or equal to the random number and the energy restriction (4) is satisfied, then a particle emission is realized. An identical procedure is followed for particle emission following two-body collisions. At higher incident energies, there may be further reduction in particle absorption due to emission from sequential multiple collisions. This, however, is not important in the energy range of our interest, and has been neglected.

In the course of evolution of the dinuclear complex, because of successive nucleon exchanges on either direction the angular momentum as well as the elementary particle and hole excitation energies in the nuclei get added up cumulatively. However, if the exchanged nucleon is finally emitted in the continuum, then it does not contribute either to the excitation energy or to the angular momentum of the recipient. The excitation energy thus generated, barring the collective energy due to the accumulation of angular momentum from particle exchange, is assumed to be thermalized at each instant. The instantaneous temperatures $T_{A,B}(t)$ are then related to the excitation energies $E^*_{A,B}(t)$ by the following relation:

$$T_{A,B}(t) = [E^*_{A,B}(t)/a]^{1/2} \ , \tag{5}$$

where the level density parameter a is taken as $M_{A,B}(t)/10$, $M_{A,B}(t)$ being the dynamical mass numbers of the reactants at any instant of time t. The dynamical change in the intrinsic nucleon momentum distribution arising out of the nonequilibrium flow of energy and momentum between the two nuclei is simulated as a finite-temperature Fermi distribution.

The exchange of nucleons causes energy and angular momentum to be transferred from the relative to the internal degrees of freedom and there is a net loss of kinetic energy and angular momentum from the entrance channel. The effect of preequilibrium emission is twofold: (i) mass, charge, energy, and angular momentum are removed from the system, and (ii) the fusion probability distribution as a function of incident angular momentum l becomes diffused and is shifted towards lower l as compared to the same obtained in the case of complete fusion [16]. Because of the stochastic nature of nucleon exchange and preequilibrium emission, mass, charge, excitation energy, and angular momentum of the incompletely fused composite as well as the primary QE and DI fragments will not have unique values. Each of these observables will have some distribution and ensemble average of any such observable $\langle X(b)\rangle$ for an impact parameter b is calculated as

$$\langle X(b)\rangle = \sum_k X_k(b)/\mathcal{N}(b) \tag{6}$$

and the probability $P_Z(b)$, for getting a fragment with charge number Z is given by

$$P_Z(b) = \sum_k \delta_{Z,Z_k}/\mathcal{N}(b), \tag{7}$$

where $\mathcal{N}(b) = N_F(b)$ for fusion reaction and $\mathcal{N}(b) = N - N_F(b)$ for non-fusion reaction; $N_F(b)$ being the total number of fused trajectories out of total N number of trajectories. The summation extends over all respective trajectories. The impact parameter dependence of $\langle X(b)\rangle$ are then approximated by appropriate analytical functions to be used in subsequent calculations.

The calculation of trajectories are done on an event-by-event basis using a Monte Carlo simulation technique

[16]. Non-fusion and fusion (complete and incomplete) events are identified from their respective trajectories. Quasielastic and deep inelastic events are further differentiated in the present calculation in the following manner. If the total kinetic-energy loss in any event is less than half of the total available energy in the center of mass [19], then the event is classified as quasielastic event, otherwise, as deep inelastic event. The primary charge distribution of the deep inelastic, quasielastic fragments and the fused composite are calculated using the following expression:

$$\sigma(Z) = 2\pi \int P_Z(b)[\mathcal{N}(b)/N] b\, db. \tag{8}$$

B. Statistical binary fragmentation phase

The primary deep inelastic, quasielastic fragments, and the incompletely fused composite formed at the end of this phase are assumed to be fully equilibrated. For fusion reaction, the incompletely fused composite has its mass ($A_{\rm IFC}$), charge ($Z_{\rm IFC}$), excitation energy ($E^*_{\rm IFC}$) and velocity ($\vec{v}_{\rm IFC}$) given by

$$\langle A_{\rm IFC}(b)\rangle = A_P + A_T - \langle N_{\rm PEP}(b)\rangle\ , \tag{9a}$$

$$\langle Z_{\rm IFC}(b)\rangle = Z_P + Z_T - \langle N^{\rm proton}_{\rm PEP}(b)\rangle\ , \tag{9b}$$

$$\langle \vec{v}_{\rm IFC}(b)\rangle = (\vec{P}_{\rm in} - \langle \vec{P}_{\rm PEP}(b)\rangle)/(m\langle A_{\rm IFC}(b)\rangle)\ , \tag{9c}$$

$$\langle E^*_{\rm IFC}(b)\rangle = E_{\rm lab} - 0.5m\langle A_{\rm IFC}(b)\rangle\langle v_{\rm IFC}(b)\rangle^2 - \langle \varepsilon_{\rm PEP}(b)\rangle, \tag{9d}$$

where $N_{\rm PEP}$ is the total number of PEP's (proton+neutron)=$N^{\rm proton}_{\rm PEP} + N^{\rm neutron}_{\rm PEP}$, A_P, Z_P, A_T, and Z_T are the mass and charge number of the projectile and the target, respectively. $\vec{P}_{\rm in}$ is the incoming momentum, $\vec{P}_{\rm PEP}$, $\varepsilon_{\rm PEP}$ are the momentum and energy carried away by PEP's and $E_{\rm lab}$ is the incident energy. For collisions not leading to fusion, the preequilibrium phase leads to the emission of DI and QE fragments with their masses, charges, and excitation energies significantly smaller compared to the case when preequilibrium emission is absent. The relevant observables corresponding to non-fusion reactions may also be calculated in a similar manner through expressions like Eq. (9).

In the second phase, the "hot" primary fragments formed at the end of the first phase undergo dynamical deformation, leading ultimately to asymmetric binary fragmentation and thereby yielding intermediate mass fragments. The statistical binary decay yields from the excited primary fragments, are governed by the conditional saddle-point potential barrier at the conditional saddle point. The partial decay width for emission of a fragment of atomic number Z from the hot composite with angular momentum l may be calculated using the transition state formalism [20],

$$\Gamma_Z(l) = [2\pi\rho_0(E^*)]^{-1} \int \rho_{\rm sad}[E_Z(l) - \varepsilon]\, d\varepsilon, \tag{10}$$

where ρ_0 (E^*) is the level density of the primary fragment of mass A_0 before decay, $\rho_{\rm sad}[E_Z(l) - \varepsilon]$ is the level density at the conditional saddle point having $B_Z(l)$ as the barrier, and ε is the kinetic energy with which the system is transiting. Integration of Eq. (10) leads to the following expression for the decay width [21]:

$$\Gamma_Z(l) = T_Z(l)\rho_{\rm sad}[E_Z(l)]/2\pi\rho_0(E^*), \tag{11}$$

where $E_Z(l) = E^* - B_Z(l)$ is the excitation energy of the fragment of atomic number Z above the barrier and $T_Z(l)$ is temperature at the conditional saddle point extracted using the relation $E_Z(l) = aT^2_Z(l)$, a being the level-density parameter. The conditional barriers have been calculated assuming the exit channel to be two diffused spheres connected by a cylindrical neck [22]. The barrier $B_Z(l)$ is calculated using the following expression [23]:

$$B_Z(l) = (M_1 + M_2 - M_0) + U_{\rm Coul} + U_{\rm prox} + [U^{\rm sad}_{\rm rot}(l) - U^0_{\rm rot}(l)], \tag{12}$$

where M_1, M_2 are the masses of the binary fragments and M_0 is the mass of the primary fragment (IFC or primary DI, QE fragments). $U_{\rm Coul}$ is the Coulomb energy between the two fragments at the conditional saddle point having surface-to-surface separation d. The nucleus-nucleus interaction is approximated by the proximity potential $U_{\rm prox}$. The last term is the difference of rotational energies between the initial ($U^0_{\rm rot}$) and final ($U^{\rm sad}_{\rm rot}$) configurations [23]. The total elemental IMF emission cross section is calculated using the expression [22]

$$\sigma(Z) = \pi\lambda^2 \sum_l (2l+1) P_F(l)\Gamma_Z(l')/\Gamma_{\rm tot}(l'), \tag{13}$$

where $P_F(l)$ is the fusion probability for angular momentum l, Γ_Z is the decay width for the element of charge Z, and $\Gamma_{\rm tot}$ ($= \Gamma_p + \Gamma_n + \Gamma_\alpha$; p, n, α refer to proton, neutron, and alpha particle, respectively) is the total decay width. The fusion probability $P_F(l)$ is defined as $P_F(l) = N_F(l)/N$, where $N_F(l)$ is the number of trajectories fused out of N trajectories for the incident angular momentum l. The fusion probabilities, calculated as a function of l, are found to be approximated by a diffuse Fermi distribution, i.e., $P_F(l) = 1/\{1 + \exp[(l - l_0)/\Delta]\}$. Using the statistical model expression [24] for level densities,

$$\rho(E^*) \propto E^{*-2} \exp[2(aE^*)^{1/2}] \tag{14}$$

we arrive at the following expression for decay width [23]:

$$\Gamma_Z(l) \propto T_Z(l)[E^*/E^*_Z(l)]^2 \times \exp\{2[aE^*_Z(l)]^{1/2} - 2(aE^*)^{1/2}\}\ . \tag{15}$$

The quantity l' in Eq. (13) is the ensemble-averaged angular momentum of the incompletely fused composite. For complete fusion, $l' = l$, but for incomplete fusion reaction, the emitted PEP's carry away some amount of angular momentum from the entrance channel and the residual angular momentum l' is generally less than l. Typically, the angular momentum of the composite l' is

found to be $\sim 0.8l$ [16]; the remaining 20% of the angular momentum is carried away by the emitted preequilibrium nucleons. Each of the decay products may further undergo successive binary fragmentation in the same manner as described above. This process stops when the excitation energy of the decaying nucleus is less than the respective conditional barrier. At each stage of fragmentation, the excitation energy and angular momentum are assumed to be shared in ratios of the masses and moments of inertia of the fragments, respectively. In the present calculation, it has been found that the excitation energy left in the system after the preequilibrium emission is not large enough and the contribution to the IMF production through successive binary decay beyond the first stage is not significant. Therefore, the statistical binary decay of the incompletely fused composite, beyond the first stage, has not been included in the present calculation.

For the QE and DI processes, we have considered only the primary projectilelike fragments. The excitation energies of these primary fragments are found to be small enough for further binary decay.

III. RESULT AND DISCUSSIONS

We have studied the IMF emission in the representative systems ^{20}Ne+^{159}Tb at 294 MeV, ^{40}Ar+^{197}Au at 1200 MeV, and ^{20}Ne+^{109}Ag at 400 and 800 MeV and have calculated relevant physical observables which have been compared with respective available experimental data.

A. Incomplete fusion: Fusion probability and excitation energy distribution

In Fig. 1 (lower half), we have plotted the fusion probability $P_F(b)$ for the incomplete fusion reactions against the impact parameter b for the systems Ar+Au at 30 MeV/u and Ne+Ag at 40 MeV/u. Fusion probability distribution for the system with higher per particle incident energy falls less sharply as compared to that of the system with lower per particle energy. This trend is similar to the one observed in our earlier work [17]. For the reaction Ne+Ag the fusion probability falls to 50% at b=2.4 fm and for the Ar+Au reaction it occurs at b=2.95 fm. The upper part of Fig. 1 shows the plot of ensemble-averaged excitation energy $\langle E^*_{\rm IFC}\rangle$ of the incompletely fused composite against impact parameter b for the reaction Ne+Ag at 800 MeV. The excitation energy is almost constant at about 300 MeV. The upward trend in the excitation energy in the region of decreasing fusion probability is due to the decrease in the preequilibrium emission with the increase in b. These fusion probabilities and excitation energies of the incompletely fused composite have been used in calculating the primary IMF yields. The calculated fusion probability distribution for the reaction Ne+Tb has a similar trend (not shown in the figure).

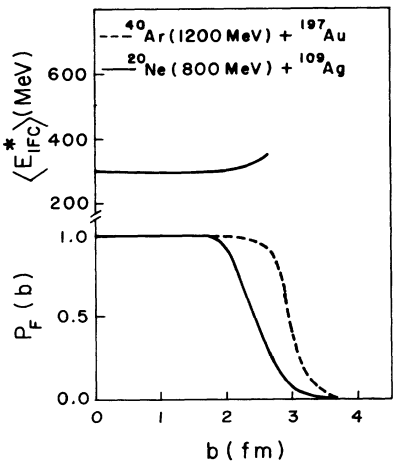

FIG. 1. Fusion probability $P_F(b)$ plotted as a function of impact parameter b (lower half) for the reactions Ne (800 MeV)+Ag (solid curve) and Ar (1200 MeV)+Au (dashed curve). Ensemble averaged excitation energy of the incompletely fused composite $\langle E^*_{\rm IFC}\rangle$ plotted as a function of b for the reaction Ne+Ag at 800 MeV (upper half).

B. Incomplete deep inelastic process

1. Energy loss and excitation energy

In deep inelastic collisions at intermediate energies, preequilibrium particles emitted at the early phase of the reaction deplete the excitation energy and the mass of the observed primary fragments. Such events are called "incomplete" deep inelastic collisions, in analogy to incomplete fusion at low-impact parameters. In Fig. 2(a), we have plotted the average energy loss $\langle E_{\rm loss}\rangle$, i.e., energy removed from the relative motion to the intrinsic

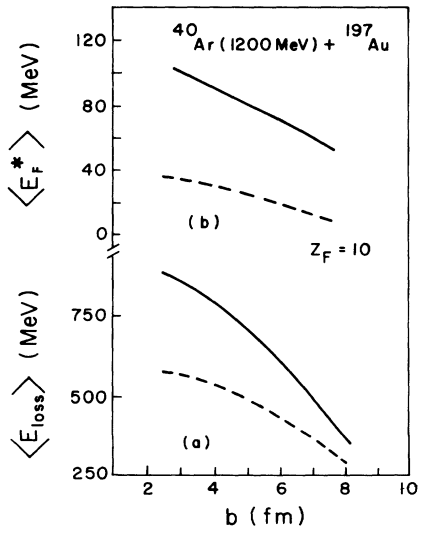

FIG. 2. (a) Average kinetic-energy loss $\langle E_{\rm loss}\rangle$ and (b) average excitation energy $\langle E^*_F\rangle$ of the fragment of charge Z_F=10 plotted as a function of impact parameter b for the reaction Ar+Au at 1200 MeV. Solid (dashed) curve corresponds to the calculation without (with) PEP emission.

excitation of the colliding partners, as function of impact parameter b for the reaction Ar (1200 MeV)+Au for two cases: (i) without preequilibrium emission (solid curve) and (ii) with preequilibrium emission (dashed curve). In the absence of preequilibrium emission the energy loss is quite high and decreases with the increasing impact parameter. This is due to the decrease in the number of particle exchange with increase in b [17]. The decrease in kinetic-energy loss when the preequilibrium emission is present may be understood as follows. The intrinsic excitations of the reactants depend upon the total number of nucleonic exchanges. An exchanged nucleon causes an elementary particle excitation in the recipient and the hole excitation in the donor nucleus. If the exchanged nucleon in the recipient is emitted in the continuum then there is no corresponding particle excitation in the recipient. Since the intrinsic excitation energy is the cumulative effect of the elementary particle and hole excitations, therefore preequilibrium emission causes net decrease in the excitation energy (i.e., kinetic-energy loss from the entrance channel) of the system by reducing the number elementary particle excitations. It is well known that with the increase in the impact parameter, the preequilibrium emission decreases and therefore the two curves gradually come closer. This is further evident from Fig. 2(b), where we have plotted the ensemble-averaged excitation energy $\langle E_F^* \rangle$ for a particular primary fragment of charge $Z_F=10$ for the case of incomplete deep inelastic process where PEP emission have been (dashed curve) and have not been (solid curve) included in the calculations.

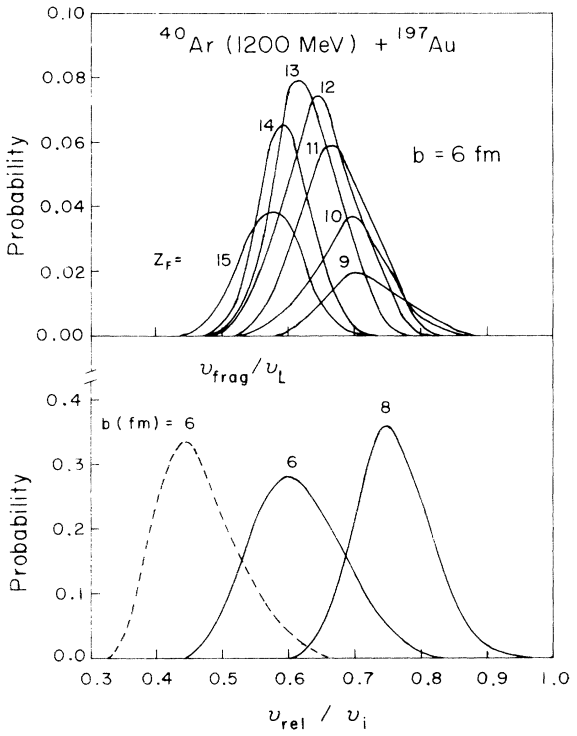

FIG. 3. Inclusive relative velocity distribution in the exit channel in Ar (1200 MeV)+Au deep inelastic collisions (lower half) plotted as a function of $v_{\rm rel}/v_i$ ($v_i, v_{\rm rel}$ being the relative velocities in the entrance and exit channels, respectively). Solid and dashed curves have the same meaning as in Fig. 2. Exclusive fragment velocity distributions (upper half) for the fragments emitted in the above reaction plotted as a function of $v_{\rm frag}/v_L$, $v_{\rm frag}$ and v_L being fragment laboratory velocity and the projectile incident velocity, respectively.

2. *Fragment velocity distribution*

In Fig. 3 (lower half) we have plotted the inclusive relative velocity distributions in the exit channel as a function of $v_{\rm rel}/v_i$, where v_i and $v_{\rm rel}$ are the relative velocities in the entrance and exit channels, respectively, for a few impact parameters for the reaction Ar+Au. The solid (dashed) curve corresponds to the calculation with (without) PEP emission. It is observed that in the case of incomplete deep inelastic collision the velocity ratio shifts to higher velocities as compared to the deep inelastic collision when there is no PEP emission. This means that the events considered to be deep inelastic in the case of no PEP emission may be termed as quasielastic in the case of incomplete deep inelastic events purely on the relative velocity considerations as the most peripheral events would be having the relative velocity close to the incident velocity in both the cases. The increase in relative velocity is a consequence of the PEP emission which, in turn, decreases the reduced mass in the exit channel. Moreover, with the increase in the impact parameter, the velocity distribution is shifted towards higher velocity. At higher impact parameters the number of nucleonic exchanges is small and therefore the energy damping is also small. This leads to the observed shift in the velocity distribution to higher relative velocities at large impact parameters. In the upper half of Fig. 3 we have plotted the exclusive velocity distributions of the fragment ($v_{\rm frag}/v_L$, $v_{\rm frag}$ and v_L being the fragment and projectile velocities in the laboratory, respectively) of various projectilelike fragments at an impact parameter b=6 fm. It is observed that the peak of the distribution moves from lower to higher velocities as one goes from heavier to lighter fragments. This may be intuitively understood in the following manner. Assuming that at a particular impact parameter the average energy loss for all the events leading to the emission of different fragments is same, the observed fact is simply a consequence of momentum conservation.

3. *Fragment charge distributions*

In Fig. 4 we have plotted fragment charge distributions at various impact parameters for the "incomplete" deep inelastic collisions [Fig. 4(a)] and for deep inelastic collisions when there is no PEP emission [Fig. 4(b)] for the system Ar+Au. It is evident from the figure that in the case of incomplete deep inelastic collisions, the peak of the charge distributions shifts to a lower value of Z_F as compared to the case when there is no PEP emission. The shift is found to be of the order of 3–4 units

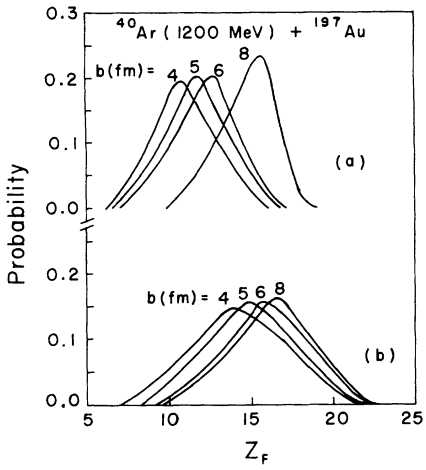

FIG. 4. Fragment charge distributions plotted as a function of fragment charge Z for Ar (1200 MeV)+Au deep inelastic collisions at impact parameters b=4, 5, 6, and 8 fm. (a) [(b)] corresponds to calculations with (without) PEP emission.

of charge except for large impact parameter where the shift is reduced to ~1 unit. At large impact parameters the number of emitted preequilibrium particles is small and this causes the reduction in the observed shift in the charge distribution.

The widths of the charge distributions in the case of incomplete deep inelastic collision are also found to be smaller than those when there is no preequilibrium emission. Intuitively, this may be understood as follows. In the evolution of the dinuclear complex nucleon exchanges take place in both directions, inwards and outwards. The inward (outward) nucleon exchange flux increases (decreases) the mass and charge of the reactants. When PEP emission is switched on a fraction of the inward flux of nucleons is emitted in the continuum. This therefore effectively reduces the net number of exchanges. As the widths of the distributions are proportional to the net number of exchanges between the reactants this causes the observed reduction in charge distribution widths. The reduction in the width is typically ~30% in this case, which is in fair agreement with a simple estimate of the same assuming the stochastic nature of nucleon exchange.

C. Elemental IMF yield distributions

The calculated intermediate mass fragment yields for the reaction ^{20}Ne+^{159}Tb at 294 MeV, ^{40}Ar+^{197}Au at 1200 MeV, and ^{20}Ne+^{109}Ag at 400 and 800 MeV bombarding energy have been plotted in Figs. 5–7, respectively along with the respective experimental data for comparison. In the following we shall be using the term deep inelastic for the incomplete deep inelastic process unless mentioned specifically.

Figure 5 shows the predicted values of the total elemental cross sections for the quasielastic and the combined deep inelastic and quasielastic processes for the reaction Ne+Tb along with the experimental data [25]. It is clear from Fig. 5 that the theoretical predictions are in

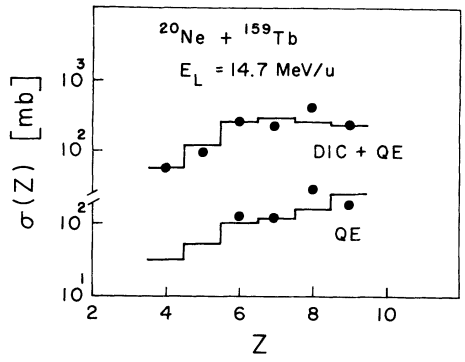

FIG. 5. Angle-integrated cross sections for QE and (DI+QE) reactions for the system ^{20}Ne+^{159}Tb at 294 MeV plotted as a function of fragment atomic number Z. Solid circles are the experimental measurements [25], and the solid histograms refer to the present theoretical predictions.

good agreement with the experimental data for both QE and (QE+DI) processes. Experimentally, the QE and DI components of the cross sections are determined from the shape of the inclusive kinetic-energy spectra of the ejectiles which exhibit double-humped structure [25]. However, at larger angles and for smaller ejectiles, these two components are not easily separable and this introduces some degree of uncertainties in the estimation of individual QE and DI components. Similarly, some uncertainty may also creep up in the theoretical estimation of QE and DI components depending on the energy-loss cutoff used in the calculation. Nevertheless, the estimation of total non-fusion (QE+DI) contribution to the IMF yield would be rather free from such ambiguities, and a good agreement achieved between the theoretical results and the experimental data in this case points to the success of the present model.

The experimental data for the deep inelastic fragment emission cross sections for the system ^{40}Ar+^{197}Au at 30 MeV/u bombarding energy [26] as well as the corresponding theoretical predictions are displayed in Fig. 6. It is seen that, except for lighter fragments (Z < 8), the present calculation is in fair agreement with the data.

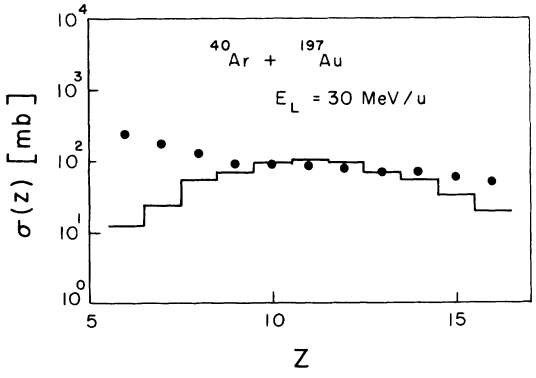

FIG. 6. Angle-integrated IMF emission cross sections as a function of fragment Z for the reaction ^{40}Ar+^{197}Au at 30 MeV/u bombarding energy. The solid histograms represent theoretical predictions and the solid circles are the experimental data [26].

The peak of the distribution appears at Z=11, which is considerably lower than the projectile Z. At intermediate energies, a number of preequilibrium nucleons are emitted as PEP's from both the projectile and the target. It is well known that, for an asymmetric target-projectile combination, the lighter of the two loses more particles on the average [10]—which explains the inward shift of the peak of the DI fragments charge distribution. The cross sections for the lighter elements ($Z < 8$) cannot be explained in terms of primary DI emission alone. However, in this case, there may be some enhancement due to successive binary decay of the heavier (targetlike) deep inelastic fragments which has not been considered in the present calculation.

In Fig. 7, the theoretical predictions and the experimental measurements [27] of total elemental cross-sections for the ^{20}Ne+^{Nat}Ag system at the incident energies of 20, 40 MeV/u as a function of fragment charge have been displayed for comparison. The dashed lines correspond to the contribution of the DI component and the solid lines represent the total (DI+binary decay of IFC) calculated cross sections. It is clear from Fig. 7 that IMF's having $Z < Z$(projectile) are emitted almost entirely through deep inelastic process, whereas the emission of IMF's with $Z > Z$(projectile) is dominated by the binary decay of the incompletely fused composite. However, the calculated yields of the fragments with Z in the range of 10–13 are underestimated. As the lighter of the reactants lose more particles in the preequilibrium phase, the non-fusion (QE and DI) processes in the present model will not contribute significantly to the fragment yield for Z larger than Z(projectile) and the discrepancy for the fragments with Z=10–13 may be due to the noninclusion of some other direct reaction channels (pickup reactions, say) in the present calculation. A good agreement between the theoretical predictions and the experimental data is achieved over the whole range of Z if contributions from both the deep inelastic process and the decay of the incompletely fused composite are properly taken into account.

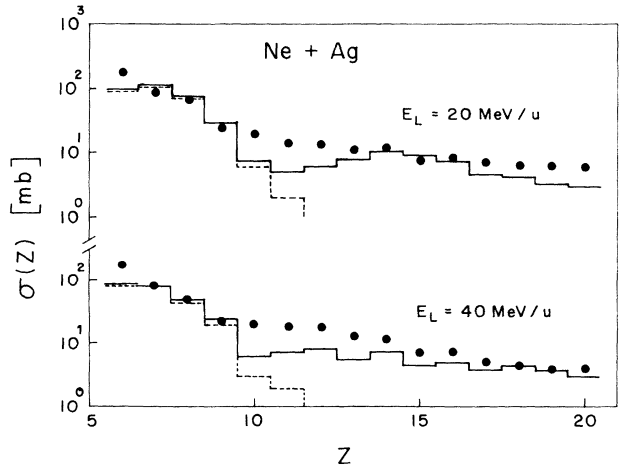

FIG. 7. Same as Fig. 2 for the system ^{20}Ne+^{nat}Ag at 20 and 40 MeV/u bombarding energy. Solid circles are the experimental data [27]. The dashed histogram is the theoretical contribution from DI process and solid histogram is the combined contribution of the DI and the fusion process.

D. Secondary deexcitation

It is evident from the above discussion that the present model without having any adjustable parameter is quite successful in explaining a wide variety of IMF emission data near the Fermi-energy domain. The predicted IMF yields presented above are those of the calculated primary fragments. The evaporative deexcitation of the primary fragments may affect the above results to some extent. However, the emission of preequilibrium particles in both fusion and non-fusion events cools the primary fragments sufficiently and thereby reduces the intrinsic excitations of the primary fragments as has been discussed earlier. Moreover, the increase in the yield of any fragment due to the evaporative secondary decay of the higher charge fragments may substantially be compensated by the secondary evaporative decay of the fragment itself and the total elemental cross section may not change significantly and the physics involved may remain the same. In order to verify the above conjecture, we chose two systems with maximum available energy i.e., (i) ^{40}Ar+^{197}Au at 1200 MeV for the non-fusion process leading to primary fragments and, (ii) ^{20}Ne+^{109}Ag at 800 MeV for the primary fragments originating from fusion process. Typical excitation energies per nucleon for the primary deep inelastic fragments for the system Ar+Au are found to be of the order of 1–1.5 MeV/nucleon (Table I). For the primary fragments emitted through binary decay of the fused composite formed in Ne+Ag reaction, the excitation energies are of the order of 2–2.5 MeV/nucleon (Table II). In Fig. 8 (lower half), we have plotted the decay probabilities $P_Z(\Delta Z)$ of the primary fragments for ΔZ=1 and ΔZ=2 decays [ΔZ is the difference of the atomic numbers between the primary fragment (parent) and its postevaporative daughter nucleus for the reaction Ar+Au]. The decay probabilities have been calculated using the code CASCADE [28]. In the upper half of Fig. 8 we have plotted the ratio of the final yield to the primary yield ($\sigma_{final}/\sigma_{prim}$) for the fragments versus the fragment

TABLE I. Ensemble-averaged mass $\langle A\rangle$ and excitation energy $\langle E^*\rangle$ of the incomplete deep inelastic primary fragments of charge Z in the reaction ^{40}Ar+^{197}Au at 30 MeV/u.

Z	$\langle A\rangle$	$\langle E^*\rangle$ (MeV)
6.0	14.7	15.30
7.0	17.8	19.00
8.0	20.1	20.80
9.0	22.6	23.20
10.0	25.9	27.90
11.0	26.0	26.92
12.0	27.2	26.85
13.0	29.0	28.67
14.0	30.5	33.85
15.0	31.6	31.60
16.0	33.3	38.10

TABLE II. Average mass $\langle A \rangle$ and excitation energy $\langle E^* \rangle$ of primary fragment of charge Z from the binary fragmentation of fused composite in the reaction ^{20}Ne+^{109}Ag at 40 MeV/u.

Z	$\langle A \rangle$	$\langle E^* \rangle$ (MeV)	Z	$\langle A \rangle$	$\langle E^* \rangle$ (MeV)
6.0	13.0	30.0	13.0	28.0	61.2
7.0	14.0	33.5	14.0	30.0	68.1
8.0	17.0	33.4	15.0	32.0	72.1
9.0	20.0	45.3	16.0	34.0	76.9
10.0	22.0	48.1	17.0	36.0	80.4
11.0	24.0	52.4	18.0	39.0	87.5
12.0	26.0	58.0	19.0	41.0	91.0

charge Z. σ_{final} has been calculated as follows:

$$\sigma_{\text{final}}(Z) = \sigma_{\text{prim}}(Z) - \sum_{\Delta Z} \sigma_{\text{prim}}(Z) P_Z(\Delta Z) + \sum_{\Delta Z} \sigma_{\text{prim}}(Z + \Delta Z) P_{Z+\Delta Z}(\Delta Z), \quad (16)$$

where $P_Z(\Delta Z)$ is the decay probability for the primary fragment of charge Z in the decay mode where it loses ΔZ amount of charge through evaporation, leading to the final fragment of charge $(Z - \Delta Z)$. From this curve it appears that σ_{final} varies at most by 10% from σ_{prim}. The decrease in the final cross section for Z=14,15 may be due to the noninclusion of the deexcitation of the primary fragments of charge greater than Z=15.

The CASCADE code has been further used to calculate the decay probabilities $P_Z(\Delta Z)$, for ΔZ=1,2,3 decays of the primary fragments obtained from the fusion events in the reaction Ne+Ag at 800 MeV. The results have been plotted in Fig. 9 (lower half) against the charge number Z. The ratio $\sigma_{\text{final}}/\sigma_{\text{prim}}$ have been plotted versus Z in the upper half of Fig. 9. Except for the strong feeding to the fragments with Z=9,10 from primary fragments with $Z > 10$, the overall fragment cross section does not change appreciably. However, this strong feeding to Ne and F fragments would decrease the dip observed in the primary fragment cross sections for these Z values. But the smallness of the primary fragment cross section will not change the results significantly. The decrease in the final cross section for the high-Z fragment, as mentioned earlier, is due to the noninclusion of the decay of the higher charge primary fragments.

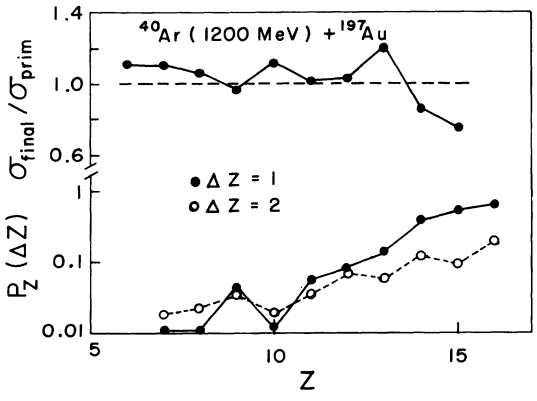

FIG. 8. Secondary decay probability $P_Z(\Delta Z)$ (lower half) and the ratio $\sigma_{\text{final}}/\sigma_{\text{prim}}$ (upper half) plotted as a function of fragment charge Z for the reaction Ar (1200 MeV)+Au. σ_{final} and σ_{prim} are as defined in the text. The lines are to guide the eye.

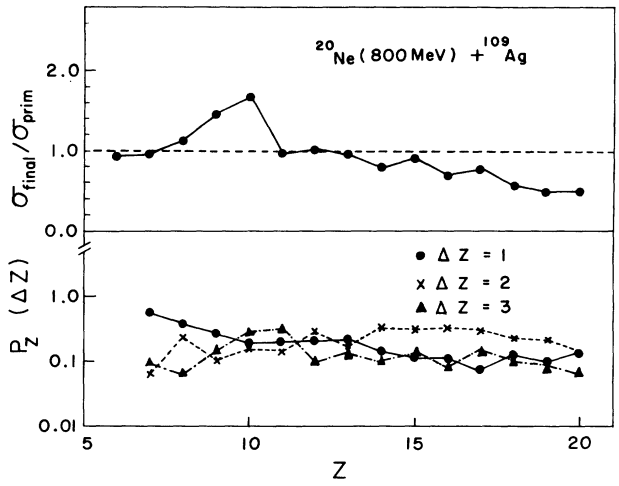

FIG. 9. Same as Fig. 8 for the system Ne (800 MeV)+Ag.

From the above discussion it is clear that the deexcitation of the primary fragments emitted either from deep inelastic collisions or from the decay of incompletely fused composite does not change the results significantly so far as elemental charge distributions are concerned. For the primary fragments originating from the QE process, the excitation energy of the fragments would be rather small compared to those originating from the deep inelastic or fusion events and as such the effect of deexcitation of the primary fragments from QE process would be still smaller. Similarly, the deexcitation of the primary fragments from low-energy reaction Ne+Tb will not be of much importance.

IV. SUMMARY AND CONCLUSIONS

In summary, we have studied the IMF yields from a few asymmetric systems with the incident energies in the Fermi-energy domain and found that the present model is quite successful in explaining a wide variety of IMF emission data. Individual contributions of the fusion and non-fusion processes to the IMF emission are quite successfully predicted by the model. In the present paper, we have made a detailed study of incomplete deep inelastic process, in particular. It has been shown that the incompleteness leads to a shift in the relative velocity distribution of DI fragments towards higher velocities. Charge distribution of DI fragments has also been observed to have shifted towards lower Z due to preequilibrium emission. In addition, the width of the charge distribution is also smaller in the case of incomplete deep inelastic process. This is due to the decrease in the net number of exchanges as a fraction of the exchange

flux is emitted in the continuum as prompt particles. In the intermediate-energy domain, PEP's carry away significant amounts of energy; therefore the primary fragments are left with less excitation energy as compared to those in the case of complete fusion. This lowers the probability of successive binary decay beyond the first stage. Therefore, successive binary decay of the primary fragments beyond the first stage have not been considered in the present calculation. The quasielastic reactions are generally dominated by a few nucleons transfer to the target. Therefore, the excitation energies of the QE fragments are not sufficiently high and as such further light charge particle evaporation from these fragments may not be quite significant [14]. In the intermediate-energy domain, deep inelastic processes are incomplete in the sense that a major fraction of the available energy is carried away by the fast particles (PEP's). As a result of the preequilibrium emission, the DI fragments are left with relatively small excitation energies compared to the situation where fast particle emission is absent. This lowers the probability of further light charge particle evaporation from the projectilelike deep inelastic fragments. Moreover, the decrease in the inclusive fragment yield due to light charge particle evaporation is more or less compensated by the feeding from the evaporative decay of the higher charge fragments. Therefore, the results of the present calculation for the inclusive elemental yield of the primary IMF's will not be significantly affected due the noninclusion of the evaporative decay of the fragments. To verify this, statistical deexcitation of the excited primaries have been studied for a few systems using the code CASCADE. It has been observed that the statistical deexcitation of the primary fragments does not affect the primary fragment yield distribution significantly.

To conclude, the present model is thus found to be quite successful in bringing out the distinctive features and estimating quantitatively the individual contributions of both fusion and non-fusion processes responsible for intermediate mass fragments emission in the intermediate-energy nucleus-nucleus collisions in an integrated manner. For asymmetric systems, the total elemental cross sections for the whole range of IMF's can be fairly well explained with this model up to the Fermi-energy domain and contribution from the true multifragmentation process, if there be any, may not be of much significance in this energy domain. However for symmetric systems in this energy domain, the excitation energies of the composite systems are quite high and there may be significant contributions to the IMF yields from processes like true multifragmentation—which are beyond the scope of the present paper.

The authors would like to thank S. K. Basu and A. Roy for their help in using the code CASCADE.

[1] S. J. Yennello, E. C. Pollacco, K. Kwiatkowski, C. Volant, R. Dayras, Y. Cassagnou, R. Legrain, E. Norbeck, V. E. Viola, J. L. Wile, and N. R. Yoder, Phys. Rev. Lett. **67**, 671 (1991).

[2] Y. D. Kim, M. B. Tsang, C. K. Gelbke, W. G. Lynch, N. Carlin, Z. Chen, R. Fox, W. G. Gong, T. Murakami, T. K. Nayak, R. M. Ronningen, H. M. Xu, F. Zhu, W. Bauer, L. G. Sobotka, D. Stracener, D. G. Sarantites, Z. Majka, V. Abenanta, and H. Griffin, Phys. Rev. Lett. **63**, 494 (1989).

[3] R. T. de Souza, L. Phair, D. R. Bowman, N. Carlin, C. K. Gelbke, W. G. Gong, Y. D. Kim, M. A. Lisa, W. G. Lynch, G. F. Peaslee, M. B. Tsang, H. M. Xu, F. Zhu, and W. A. Friedman, Phys. Lett. B **268**, 6 (1991).

[4] R. J. Charity, M. A. McMahan, G. J. Wozniak, R. J. McDonald, L. G. Moretto, D. G. Sarantites, L. G. Sobotka, G. Guarino, A. Pantaleo, L. Fiore, A. Gobbi, and K. D. Hildenbrand, Nucl. Phys. **A483**, 371 (1988).

[5] Y. Nagame, H. Ikezoe, S. Baba, K. Hata, T. Sekine, S. Ichikawa, M. Magara, K. Ideno, A. Yokoyama, Y. Hatsukawa, and T. Ohtsuki, Nucl. Phys. **A510**, 518 (1990).

[6] W. A. Friedman, Phys. Rev. C **40**, 2055 (1989).

[7] J. J. Molitoris, H. Stocker, and B. L. Winer, Phys. Rev. C **36**, 220 (1987).

[8] M. Colonna, N. Colonna, A. Bonasera, and M. DiToro, Nucl. Phys. **A541**, 295 (1992).

[9] J. Aichelin and H. Stocker, Phys. Lett. B **176**, 14 (1986).

[10] H. Morgenstern, W. Bohne, K. Grabisch, D. G. Kovar, and H. Lehr, Phys. Lett. **113B**, 463 (1982).

[11] J. Galin, H. Oeshler, S. Song, B. Borderie, M. F. Rivet, I. Forest, R. Bimbot, D. Gardes, B. Gatty, H. Guillemot, M. Lefort, B. Tamain, and X. Tarrgo, Phys. Rev. Lett. **48**, 1787 (1982).

[12] E. Holub, D. Hilscher, G. Ingold, U. Jahnke, H. Orf, H. Rossner, W. P. Zank, W. U. Schroeder, H. Gemmeke, K. Keller, L. Lassen, and W. Lucking, Phys. Rev. C **33**, 143 (1986).

[13] B. A. Remington, G. Caskey, A. Galonsky, C. K. Gelbke, L. Heilbronn, J. Heltsley, M. B. Tsang, F. Deak, A. Kiss, Z. Seres, J. Kasagi, and J. J. Kolata, Phys. Rev. C **34**, 1685 (1986).

[14] C. Block, W. Benenson, A. I. Galonsky, E. Kashy, J. Heltsley, L. Heilbronn, M. Lowe, R. J. Radtke, B. Remington, J. Kasagi, and D. J. Morrissey, Phys. Rev. C **37**, 2469 (1988).

[15] J. C. Steckmeyer, G. Bizard, R. Brou, P. Eudes, J. L. Laville, J. B. Natowitz, J. B. Patry, B. Tamain, A. Thiphagne, H. Doubre, A. Peghaire, J. Peter, E. Rosato, J. C. Adloff, A. Kamili, G. Rudolf, F. Scheibling, F. Guilbault, C. Lebrun, and F. Hanappe, Nucl. Phys. **A500**, 372 (1989).

[16] K. Krishan, S. Bhattacharya, J. N. De, and S. K. Samaddar, Nucl. Phys. **A542**, 159 (1992).

[17] S. Bhattacharya, K. Krishan, J. N. De, and S. K. Samaddar, Phys. Rev. Lett. **62**, 2589 (1989).

[18] S. Bhattacharya, C. Bhattacharya, and K. Krishan, *Proceedings of the Conference of Medium and High Energy Nuclear Physics*, Calcutta, India, 1991 (World Scientific, Singapore, 1992), p. 221.

[19] R. Bass, *Nuclear Reactions with Heavy Ions* (Springer-Verlag, Berlin, 1980), p. 256.

[20] L. G. Moretto, Nucl. Phys. **A247**, 211 (1975).

[21] L. G. Moretto and G. J. Wozniak, Prog. Part. Nucl. Phys. **21**, 401 (1988).

[22] C. Bhattacharya and S. Bhattacharya, Phys. Rev. C **43**, 1491 (1991).

[23] L. G. Sobotka, M. L. Padgett, G. J. Wozniak, G. Guarino, A. J. Pacheco, L. G. Moretto, Y. Chan, R. G. Stokstad, I. Tserruya, and S. Wald, Phys. Rev. Lett. **51**, 2187 (1983).

[24] A. Bohr and B. Mottelson, *Nuclear Structure* (Benjamin, New York, 1969), Vol. I.

[25] B. Kotlinski, H. W. Wilschut, P. C. N. Crouzen, H. Kaper, E. E. Koldenhof, H. K. W. Leegte, R. H. Siemssen, and Y. X. Xie, Nucl. Phys. **A526**, 303 (1991).

[26] U. Milkau, E. Berdermann, B. Berthier, P. Bouissou, C. Cerruti, A. Demeyer, E. M. Eckert, D. Guinet, K. D. Hildenbrand, J. Hubele, G. Imme, P. Kreutz, A. Kuhmichel, G. J. Kunde, S. Leray, P. Lhenoret, R. Lucas, U. Lynen, C. Mazur, W. F. J. Muller, C. Ngo, C. H. Pinkenburg, J. Pochodzalla, H. J. Rabe, G. Reciti, M. Ribrag, H. Sann, H. Stelzer, E. Tomasi, W. Trautmann, R. Trockel, and R. Wada, Phys. Rev. C **44**, 1242 (1991).

[27] N. H. Papadakis, N. P. Vodinas, Y. Cassagnou, R. Dayras, R. Fonte, G. Imme, R. Legrain, A. D. Panagiotou, E. G. Pollacco, G. Reciti, L. Rodriguez, F. Saint-Laurent, M. G. Saint-Laurent, and N. Saunier, Phys. Lett. B **240**, 317 (1990).

[28] F. Puhlhofer, Nucl. Phys. **A280**, 267 (1977).